https://doi.org/10.5194/egusphere-2025-1210
Preprint. Discussion started: 25 March 2025

Quantifying the impact of solar zenith angle, cloud optical thickness, and surface albedo on the solar radiative effect of Arctic low-level clouds over open ocean and sea ice

Sebastian Becker, André Ehrlich, Michael Schäfer, and Manfred Wendisch
Leipzig Institute for Meteorology (LIM), Leipzig University, Leipzig, Germany
Correspondence: Sebastian Becker (sebastian.becker@uni-leipzig.de)

Abstract. Due to their complex interactions with surface albedo, aerosol particles, and water vapour, clouds play one of the most uncertain roles in the Arctic climate system. Consequently, the cloud radiative effect (CRE), which is a quantitative measure of the impact of clouds on the radiative energy budget (REB), is subject to considerable uncertainty. To reduce this uncertainty and better understand the importance of the driving processes, it is crucial to quantitatively disentangle the various cloud and non-cloud factors that non-linearly affect the CRE. Therefore, this study uses a combination of a CRE parameterization and low-level airborne REB observations to quantify the impact of concurrently observed cloud optical thickness, solar zenith angle, and surface albedo on the solar CRE at the surface. Based on a case study characterized by inhomogeneous cloud and surface conditions in the marginal sea ice zone, the contributions of surface albedo and cloud optical thickness to the solar CRE are derived similar to the approximated partial radiative perturbation technique applied in climate dynamics. It is shown that the surface albedo contributed more than 95 % to the solar CRE difference between open ocean and sea ice. Using the same approach, the analysis was extended to observations from a series of aircraft campaigns, indicating that the non-cloud conditions frequently dominate seasonal and surface-type differences of the solar CRE.

1 Introduction

The increase of the Arctic near-surface temperature is proceeding at least twice as fast compared to global average values (Wendisch et al., 2023) and illustrates a drastic change of the Arctic climate system. This rapid transformation results from multiple Arctic-specific processes and feedback mechanisms (e. g., Goosse et al., 2018), amplifying the initial climate warming (Serreze and Barry, 2011; Wendisch et al., 2023). Beside Arctic warming, a second obvious indicator of this so-called Arctic amplification is the pronounced decline of the Arctic sea ice, which is particularly prominent during the annual minimum of sea ice extent in September. With respect to the average sea ice extent of the period 1991–2020, Meier et al. (2022) reported a decline of 14 % per decade in September, while only 3 % per decade were observed in March. The corresponding expansion of open ocean areas causes direct and indirect changes of the radiative energy budget (REB) at the surface. On the one hand, the darker open ocean directly increases the absorption of solar radiation, leading to a larger solar REB and intensifying the surface warming (surface albedo feedback; e. g., Hall, 2004). On the other hand, stronger upward moisture fluxes over open ocean enhance the formation of clouds (Vavrus et al., 2011), which belong to the most important modulators of the REB. While

https://doi.org/10.5194/egusphere-2025-1210
Preprint. Discussion started: 25 March 2025

this second effect does not play a significant role in summer, cloudiness will increase considerably in autumn (Morrison et al., 2019), concurrent with the strongest sea ice retreat.

Low-level clouds play a complex role in the Arctic climate system (Wendisch et al., 2019) and their impact on the REB at the surface or the top of the atmosphere (TOA) is defined by the cloud radiative effect (CRE) following Ramanathan et al. (1989):

$$\mathrm{CRE} = F_{\mathrm{net,cld}} - F_{\mathrm{net,cf}} \tag{1}$$

$$= (F^{\downarrow}_{\mathrm{cld}} - F^{\uparrow}_{\mathrm{cld}}) - (F^{\downarrow}_{\mathrm{cf}} - F^{\uparrow}_{\mathrm{cf}}). \tag{2}$$

The net irradiances $F_{\mathrm{net,cld}}$ and $F_{\mathrm{net,cf}}$ in Eq. 1 quantify the REB in cloudy and cloud-free conditions and are defined as the difference of the respective downward ($F^{\downarrow}_{\mathrm{cld}}$, $F^{\downarrow}_{\mathrm{cf}}$) and upward ($F^{\uparrow}_{\mathrm{cld}}$, $F^{\uparrow}_{\mathrm{cf}}$) irradiances. While the CRE in the solar spectral range is mostly negative (cooling effect), clouds generally exert a warming effect in the thermal-infrared (TIR) spectral range of atmospheric radiation. The sign of the total (solar plus TIR) CRE depends on the balance of both components. Due to this antagonism, the feedback of clouds represents a key source of uncertainty in climate projections (Forster et al., 2021). Challenges related to the cloud feedback arise from non-linear interactions of clouds with, e. g., surface, aerosol particles, or water vapour, which affect the CRE and propagate into other feedback mechanisms (Choi et al., 2020; Kay et al., 2016). In the past, the cloud feedback was often quantified by the change in CRE between two climate states (e. g., Cess et al., 1990). However, Soden et al. (2004) demonstrated that this approach does not yield an accurate estimate of cloud feedback, because the CRE can change due to non-cloud properties although the cloud characteristics are unchanged. In fact, negative CRE changes often coincide with positive cloud feedback. A common approach to correct the CRE change for the non-cloud contributions is to subtract the cloudy (total minus cloud-free) portions of the non-cloud feedbacks (Soden et al., 2008; Shell et al., 2008). Despite the available solutions, the uncertainty resulting from cloud-radiative processes and the insufficient representation of complex cloud-involving interactions in climate models require a characterization of the CRE and a separation of the impacts of different cloud and non-cloud properties on the CRE.

Several studies have investigated the seasonal cycle of the CRE at the surface using ground-based observations over mostly snow- and ice-covered surfaces across the Arctic (e. g., Intrieri et al., 2002; Miller et al., 2015; Ebell et al., 2020). In contrast to lower latitudes, all studies in the Arctic identified a total warming effect of clouds on annual average, turning into a cooling effect during summer with decreasing solar zenith angle (SZA) and surface albedo. Becker et al. (2023) compared the surface CRE obtained from low-level airborne measurements over adjacent sea ice and open ocean surfaces during three, seasonally distinct campaigns and found a strong solar cooling effect over open ocean due to the low surface albedo. The TIR CRE is less affected by seasonal variability, as the increased emission by clouds for warmer temperatures is often compensated by stronger water vapour absorption below the cloud (Cox et al., 2015; Becker et al., 2023).

Despite these studies, a quantitative analysis of the impact of important drivers on the CRE variability is largely lacking; existing research rather focused on the surface REB. Di Biagio et al. (2012) used a combination of measurements and results from radiative transfer simulations to disentangle the contributions of water vapour, aerosol particles, and multiple scattering from the downward solar irradiance measured at Pituffik Space Base (formerly Thule Air Base), Greenland during cloud-free

https://doi.org/10.5194/egusphere-2025-1210
Preprint. Discussion started: 25 March 2025

conditions. They concluded that water vapour usually dominates the solar downward irradiance in cloud-free conditions. Jäkel et al. (2024, submitted to J. Eur. Meteorol. Soc.) analyzed the relative impact of SZA, cloud total water path, and surface albedo on the variability of the solar surface REB over the course of the summer season using Arctic-wide simulations. Applying two regression methods, they identified the SZA to exert the largest impact outside the Central Arctic, while in the Central Arctic the dominant contributor depended on the melting stage.

To estimate sensitivities of the surface CRE with respect to cloud, surface, and thermodynamic conditions, Shupe and Intrieri (2004) applied a simple CRE parameterization and measurements obtained during the shipborne Surface Heat Budget of the Arctic Ocean drift expedition (SHEBA, Uttal et al., 2002). However, these sensitivity estimates do not account for interactions between the parameters. In the present study, a similar parameterization is used in combination with airborne irradiance measurements to quantitatively partition concrete changes of solar CRE into its contributions of SZA, surface albedo, and cloud optical thickness, including the partitioning of interaction terms. Since the TIR CRE is not considered in this study, the term CRE refers explicitly to the solar surface CRE in the following. The measurements and the applied CRE parameterization are described in Sect. 2. The investigations are demonstrated for a case with inhomogeneous cloud and surface conditions, which both affect the evolution of the CRE. Section 3 introduces the case study and disentangles the relative impacts of the drivers on the CRE evolution along the continuous transition across the sea ice edge during this case. However, separating these impacts is not limited to cases with a continuous transition. Based on a method similar to a technique used in climate dynamics, Sect. 4 quantifies the relative contributions to a CRE difference between two distinct states, such as different seasons or locations. To demonstrate this approach, the relative contributions of surface albedo and cloud optical thickness are calculated for the CRE contrast between open ocean and sea ice of the example case in Sect. 4.1. In Sect. 4.2, this quantitative method is then applied to cases of CRE contrast between different campaigns and surface types to extend the qualitative analysis by Becker et al. (2023).

2 Observations and solar CRE parameterization

2.1 Solar radiation measurements and simulations

The measurements used for this study were obtained in the vicinity of Svalbard during two airborne campaigns, covering different seasons. The Arctic CLoud Observations Using airborne measurements during polar Day campaign (ACLOUD) took place in May/June 2017 (Wendisch et al., 2019; Ehrlich et al., 2019), while the Airborne measurements of radiative and turbulent FLUXes of energy and momentum in the Arctic boundary layer campaign (AFLUX) was performed in March/April 2019 (Mech et al., 2022). Both campaigns deployed the research aircraft *Polar 5* from Alfred Wegener Institute, Helmholtz Centre for Polar and Marine Research (AWI), which was equipped with an instrumental payload to acquire turbulence, radiation, and cloud remote sensing data. Cloud microphysical properties were derived from cloud in-situ probes onboard *Polar 5* during AFLUX and the additionally deployed AWI aircraft *Polar 6* during ACLOUD.

The surface CRE was retrieved from a combination of radiation measurements and radiative transfer simulations. During low-level flight sections, $F^{\downarrow}_{\mathrm{cld}}$ and $F^{\uparrow}_{\mathrm{cld}}$ were measured by broadband Kipp&Zonen CMP-22 pyranometers attached to the

https://doi.org/10.5194/egusphere-2025-1210
Preprint. Discussion started: 25 March 2025

aircraft and corrected for aircraft attitude and instrument inertia (Ehrlich et al., 2019). From these observations, the surface albedo α and $F_{\mathrm{net,cld}}$ were derived. To obtain $F_{\mathrm{cf}}^{\downarrow}$, radiative transfer simulations were performed with the radiative transfer code *uvspec*, which is incorporated in the library for radiative transfer (*libradtran*, Emde et al., 2016). The simulations were initialized with the local SZA calculated from time and position of the aircraft, the measured values of α, and the observed thermodynamic profile of temperature and relative humidity. The thermodynamic observations resulted from adjacent aircraft ascents and descents as well as from close-by radiosoundings for higher altitudes.

Further data relevant for the analysis include the sea ice concentration (SIC) and the cloud optical thickness τ along the flight track. The SIC was derived from imagery of a downward-looking digital camera equipped with a 180° fish-eye lens based on a sea ice mask (Perovich et al., 2002). To obtain τ, a look-up table of simulated $F_{\mathrm{cld}}^{\downarrow}$ created as a function of SZA, α, and τ was applied to the local observations of SZA, α, and $F_{\mathrm{cld}}^{\downarrow}$ (Stapf et al., 2020). All relevant data are published in Stapf et al. (2021).

2.2 Parameterization of solar CRE

The quantitative investigation of the impact of different drivers on the CRE requires a relationship between CRE and cloud and surface properties. Therefore, α in cloudy conditions as well as the transmissivities of cloud $\mathcal{T}_{\mathrm{cld}}$ and cloud-free atmosphere $\mathcal{T}_{\mathrm{atm}}$ are introduced and obtained from the irradiance measurements and simulations described in Sect. 2.1:

$$\alpha = \frac{F_{\mathrm{cld}}^{\uparrow}}{F_{\mathrm{cld}}^{\downarrow}}, \tag{3}$$

$$\mathcal{T}_{\mathrm{cld}} = \frac{F_{\mathrm{cld}}^{\downarrow}}{F_{\mathrm{cf}}^{\downarrow}}, \tag{4}$$

$$\mathcal{T}_{\mathrm{atm}} = \frac{F_{\mathrm{cf}}^{\downarrow}}{F_0 \cdot \mu}. \tag{5}$$

The denominator in Eq. 5 describes the downward irradiance at the TOA, where $F_0 = 1361\,\mathrm{W\,m^{-2}}$ represents the solar constant and μ is the cosine of the SZA.

To describe the impact of clouds on the CRE, $\mathcal{T}_{\mathrm{cld}}$ is not a suited quantity, because it is a function α and μ in addition to the independent cloud property τ. The intensified multiple reflection over brighter surfaces causes $\mathcal{T}_{\mathrm{cld}}$ of the same cloud to be higher over sea ice than over open ocean. Therefore, $\mathcal{T}_{\mathrm{cld}}(\mu, \tau, \alpha)$ is expressed by the model-based parameterization of Fitzpatrick et al. (2004), with:

$$\mathcal{T}_{\mathrm{cld}}(\mu, \tau, \alpha) = \frac{a(\tau) + b(\tau) \cdot \mu}{1 + (c - d \cdot \alpha) \cdot \tau}. \tag{6}$$

The functions $a(\tau)$ and $b(\tau)$ in Eq. 6 are given by:

$$a(\tau) = a_1 + (1 - a_1) \cdot \exp(-k_1 \cdot \tau), \tag{7}$$

$$b(\tau) = b_1 \cdot \left[1 + b_2 \cdot \exp(-k_2 \cdot \tau) + b_3 \cdot \exp(-k_3 \cdot \tau)\right], \tag{8}$$

while a_1, b_i, c, d, and k_i ($i = 1, 2, 3$) in Eqs. 6–8 are coefficients listed in Table 1 that are valid for an effective cloud droplet radius of 8.6 µm (Fitzpatrick et al., 2004). Droplets of this scale are typical for Arctic low-level clouds (Mioche et al., 2017)

https://doi.org/10.5194/egusphere-2025-1210
Preprint. Discussion started: 25 March 2025

Table 1. Coefficients used in Eqs. 6–8 for the parameterization of $\mathcal{T}_{\mathrm{cld}}$ (Fitzpatrick et al., 2004).

a_1	b_1	b_2	b_3	k_1	k_2	k_3	c	d
0.58	0.74	−0.1612	−0.8343	1.9785	0.2828	2.3042	0.1365	0.1291

and deviations from this droplet size bias the parameterized $\mathcal{T}_{\mathrm{cld}}$ by less than 2 % (Fitzpatrick et al., 2004). Similar to $\mathcal{T}_{\mathrm{cld}}$, the surface albedo α is affected by cloud–surface interactions and changes as a function of μ and τ (e. g., Stapf et al., 2020). However, parameterizations of cloud transmissivity (Fitzpatrick et al., 2004) and surface albedo (Gardner and Sharp, 2010; Jin et al., 2011) suggest that the surface albedo difference between a cloud-free and an opaque-cloud case is weaker than the difference in cloud transmissivity between sea ice and open ocean. Therefore, the change in α between cloudy and cloud-free conditions is neglected in this study.

Provided that α is equal in cloudy and cloud-free conditions, inserting Eqs. 3–5 into Eq. 2 and replacing $\mathcal{T}_{\mathrm{cld}}$ by the parameterization of Eq. 6 yields an expression for the solar CRE that is dependent on $\mathcal{T}_{\mathrm{atm}}$, μ, τ, and α. This expression reads:

$$\mathrm{CRE}(\mu,\tau,\alpha) = F_0 \cdot \mathcal{T}_{\mathrm{atm}} \cdot \mu \cdot \mathcal{T}_{\mathrm{cld}}(\mu,\tau,\alpha) - F_0 \cdot \mathcal{T}_{\mathrm{atm}} \cdot \mu \cdot \mathcal{T}_{\mathrm{cld}}(\mu,\tau,\alpha) \cdot \alpha - F_0 \cdot \mathcal{T}_{\mathrm{atm}} \cdot \mu + F_0 \cdot \mathcal{T}_{\mathrm{atm}} \cdot \mu \cdot \alpha, \tag{9}$$

and is identical to the parameterization used by Shupe and Intrieri (2004, their Eq. 5). For $\mathcal{T}_{\mathrm{atm}}$, a constant value of 0.75 is assumed, corresponding to the mean value of all observations collected during AFLUX and ACLOUD in cloudy conditions with τ larger than 1.125 (this threshold corresponds to a liquid water path of 5 g m^{-2} assuming an effective droplet radius of 8 µm). This assumption is justified by the excellent correlation between the observed and the parameterized CRE (Eq. 9) that is demonstrated by Fig. 1 as a two-dimensional frequency distribution. The coefficient of determination R^2 is 0.9939 and indicates a sufficient accuracy of the CRE parameterization. This proper agreement is due to the fact that both the CRE and the regressors were largely retrieved from the same irradiance quantities. Minor deviations are primarily caused by the variation of $\mathcal{T}_{\mathrm{atm}}$ between 0.63 and 0.82, which, similar to $\mathcal{T}_{\mathrm{cld}}$, depends on μ, α, and the optical thickness of the cloud-free atmosphere that is affected by aerosols and trace gases. However, the following quantification of the drivers' impact on the CRE is hardly limited by the applied assumptions.

3 Relative contributions for continuous observations

3.1 Case study

The approach to disentangle the impact of various drivers on a continuous transition of the CRE is demonstrated for a case study, which is based on a flight section with variable cloud and surface conditions performed during AFLUX on 4 April 2019. The basic weather situation during this flight is illustrated in Fig. 2. Both at the surface and the 850 hPa pressure level, a low-pressure system was located north-west of the Fram Strait, while high pressure was present towards south-east. At the surface, this constellation caused a southerly advection of warm air west of Svalbard, while south-westerly wind at 850 hPa

https://doi.org/10.5194/egusphere-2025-1210
Preprint. Discussion started: 25 March 2025

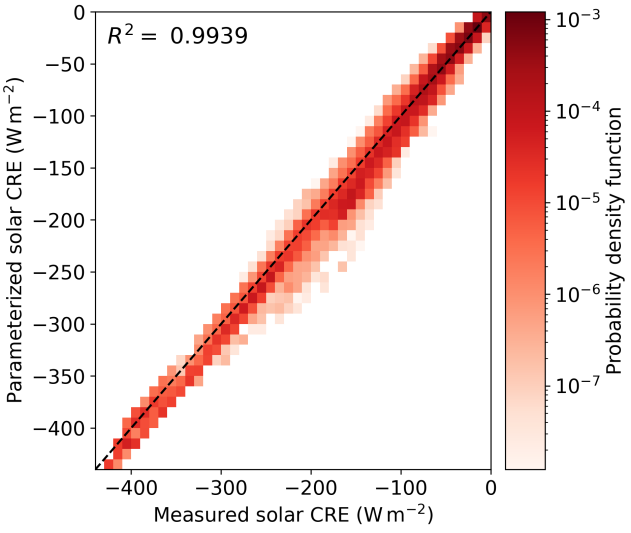

Figure 1. Two-dimensional probability density function depending on parameterized solar CRE (Eq. 9) and observed solar CRE considering all cloudy observations (τ larger than 1.125) of AFLUX and ACLOUD. The dashed line marks the 1:1-line.

pushed a cloud with inhomogeneous optical thickness over the sea ice edge (Fig. 2). Roughly parallel to the 850 hPa isohypses and across the sea ice edge, a flight leg was set up that was flown four times by *Polar 5* in different altitudes. The second leg, headed from north-east to south-west, was performed at low altitude and offered the subset of observations used for the analysis of this example case.

Figure 3a illustrates the evolution of μ, τ, and α (right y-axes) along the low-level flight leg as a function of the geographic latitude. To reduce small-scale variability, all time series are smoothed with a two-minute Hann window. The corresponding SIC is shown in Fig. 3b. The SZA (μ) varied only weakly between 74° (0.276) at the south-western and 75.3° (0.254) at the north-eastern end of the flight leg. In contrast, the variability of α and τ was substantial. The surface albedo increased from values less than 0.1 over open ocean to almost 0.9 over sea ice with an enhanced variability in the marginal sea ice zone (MIZ). The cloud optical thickness roughly ranged between 5 and 40 and the optically thickest clouds were observed in the central part of the flight leg. Beside this intermediate cloud thickening, τ was higher and ranged up to 22 over open ocean, while it did not exceed 10 over sea ice.

Due to the weak variability of the SZA indicated by Fig. 3a, the impact of the SZA on the CRE can be neglected in the present case study. Therefore, μ in Eq. 9 is fixed to its mean value along the low-level flight leg $\bar{\mu} = 0.264$ (SZA $= 74.7°$). Additionally, $\mathcal{T}_{\mathrm{atm}}$ is adjusted to the mean value resulting from this subset of observations only and corresponds to 0.72. The calculated CRE is represented by the black line in Fig. 3a and well resembles the observed CRE (red line) with $R^2 = 0.9978$.

https://doi.org/10.5194/egusphere-2025-1210
Preprint. Discussion started: 25 March 2025

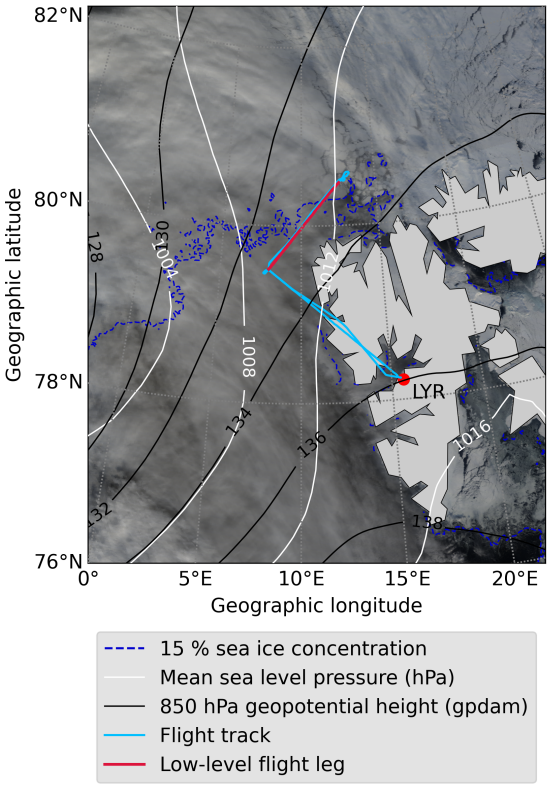

Figure 2. True-colour satellite image (composite of MODIS channels 1, 4, and 3) observed on 4 April 2019, 10:15 UTC and overlaid by mean sea level pressure and 850 hPa geopotential from ERA5 reanalysis (Hersbach et al., 2020), and the 15 % isoline of satellite-derived sea ice concentration (Spreen et al., 2008). Additionally, the flight track and the low-level flight leg are highlighted.

3.2 Method and application to the case

For the continuous observations along the flight leg of the example case (Fig. 3a), the instantaneous change of the CRE is quantified by the total differential of Eq. 9, which reads:

$$\frac{\mathrm{dCRE}}{\mathrm{d}t} = S_\tau(\tau,\alpha)\cdot\frac{\mathrm{d}\tau}{\mathrm{d}t} + S_\alpha(\tau,\alpha)\cdot\frac{\mathrm{d}\alpha}{\mathrm{d}t}. \tag{10}$$

The terms on the right hand side of Eq. 10 represent the absolute contributions of τ and α to the CRE change per unit of time t, which are determined by both the sensitivities of the CRE with respect to τ (S_τ) and α (S_α) and the absolute temporal change of these parameters (temporal derivatives in Eq. 10). The sensitivity coefficients are given by:

$$S_\tau(\tau,\alpha) = \frac{\partial \mathrm{CRE}}{\partial \tau}, \tag{11}$$

$$S_\alpha(\tau,\alpha) = \frac{\partial \mathrm{CRE}}{\partial \alpha}, \tag{12}$$

https://doi.org/10.5194/egusphere-2025-1210
Preprint. Discussion started: 25 March 2025

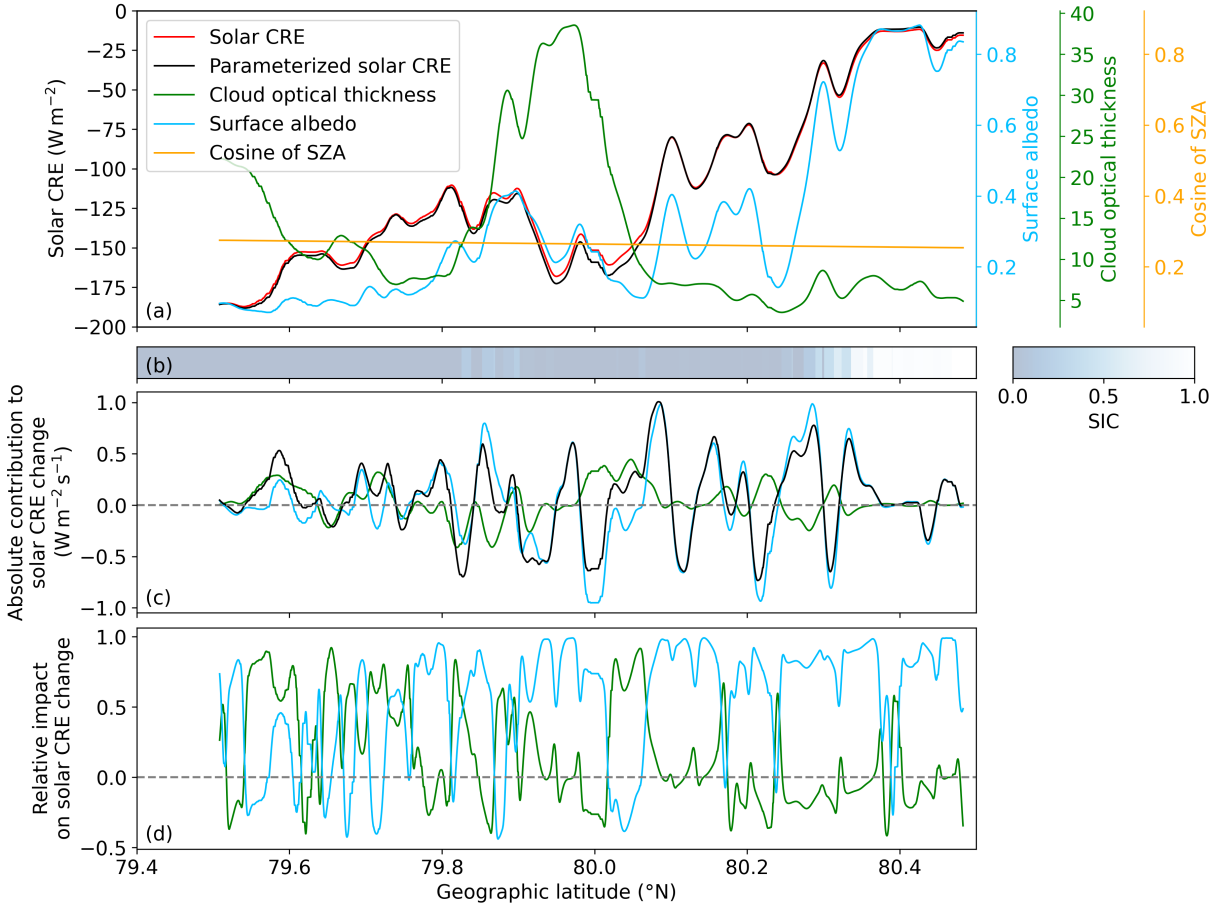

Figure 3. Evolution of (a) observed and parameterized (Eq. 9) solar CRE (left y-axis) as well as μ, τ and α (right y-axes) smoothed with a 2-minute Hann window, and (b) sea ice concentration (SIC) along the low-level flight leg as a function of geographic latitude. Time series of (c) temporal solar CRE gradient (black) as well as its absolute contributions of τ and α, and (d) the relative impact of τ and α to the solar CRE change. The time series in (d) are additionally smoothed with a 30-second Hann window. See text for more details.

and discussed in detail in Appendix A. The results of the separated contributions are shown in Fig. 3. The absolute contributions of τ and α illustrated in Fig. 3c indicate their respective tendency to the CRE transition. The precise calculation of relative contributions of τ and α as the ratio of these tendencies to the CRE change fails when the latter approaches zero. Therefore, the relative impacts shown in Fig. 3d are calculated as the absolute contributions relative to the sum of the magnitudes of all absolute contributions. The positive or negative sign indicates whether a relative impact agrees with or opposes the CRE change, respectively. This measure is assured to not exceed 1 in magnitude. Nevertheless, peaks with short periods of sign conversion still occur in the neighbourhood of zeros of the CRE change and require an additional smoothing with a 30-second Hann window.

https://doi.org/10.5194/egusphere-2025-1210
Preprint. Discussion started: 25 March 2025

The generally decreasing τ south of 79.7° N and between 80.0° and 80.1° N caused a positive tendency to the CRE at most points, while the intermediate increase of τ tended to mostly decrease the CRE (green line in Fig. 3c). North of 80.1° N, where τ was rather constant, its contribution fluctuated between positive and negative tendencies depending on the exact gradient, but revealed only a small value on average. Likewise, the surface albedo contribution (blue line in Fig. 3c) oscillated around zero over open ocean, but showed more persistent periods of positive and negative tendencies to the CRE in the MIZ between 79.8° and 79.9° N and between 79.9° and 80.05° N, respectively. Towards the sea ice, the variable but broadly increasing α resulted in a fluctuating contribution with a positive tendency on average.

From Fig. 3d, it is obvious that the CRE change was mostly controlled by the evolution of τ over open ocean, where the rather low surface albedo change caused only small positive or negative impacts. In contrast, α largely drove the CRE as soon as the MIZ was reached. North of 80.1° N, the CRE change in Fig. 3c basically follows the contribution term of α due to the weak cloud variability. Despite the intensive cloud thickening, τ did not significantly affect the CRE in the central part of the leg due to the weak sensitivity of the CRE on τ for optically thick clouds. Only towards the end of the following cloud thinning between 80.0° and 80.05° N, τ briefly dominated the CRE change.

4 Relative contributions between states

To retrieve relative contributions between two distinct states without a close spatial or temporal correlation, differentiating the CRE as in Eq. 10 is not a suited method. Nevertheless, the CRE contrast between these states similarly results from the combined change of the drivers. To disentangle their respective impacts, this section presents a method that is similar to the so-called partial radiative perturbation (PRP) technique used in climate dynamics to separate feedback mechanisms (Wetherald and Manabe, 1988). The PRP method quantifies the contribution of a feedback to the REB difference between two simulated climate states by means of radiative transfer simulations, where only the variables associated with the respective feedback are changed and all other variables are held constant. For the solar REB, Taylor et al. (2007) proposed a simplified approximated PRP (APRP), using a parameterization instead of a full radiative transfer simulation to calculate the REB. In the present study, REB and climate feedbacks are replaced by the CRE and its drivers and the CRE parameterization is given by Eq. 9.

4.1 Method based on case study

The applied method is demonstrated for the case study introduced in Sect. 3.1. Figure 4 illustrates the CRE calculated from Eq. 9 as a function of τ and α. The two highlighted states are defined by the median values obtained from the observations over open ocean (SIC less than 5 %) and sea ice (SIC larger than 95 %). These median values of τ and α amount to 8.5 and 0.10 over open ocean (dot in Fig. 4) and 7.0 and 0.78 over sea ice (cross in Fig. 4). With a stronger cooling effect for higher τ and lower α, the calculated CRE over open ocean and sea ice are $-144.2\,\mathrm{W\,m^{-2}}$ and $-11.9\,\mathrm{W\,m^{-2}}$, respectively. These values compare well to the observed median CRE values of $-144.3\,\mathrm{W\,m^{-2}}$ and $-13.3\,\mathrm{W\,m^{-2}}$ and produce a CRE difference of $\Delta\mathrm{CRE} = 132.3\,\mathrm{W\,m^{-2}}$.

https://doi.org/10.5194/egusphere-2025-1210
Preprint. Discussion started: 25 March 2025

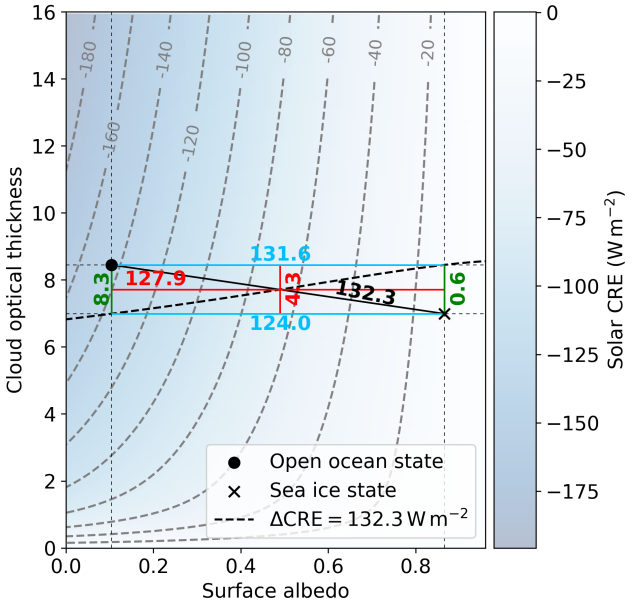

Figure 4. Solar CRE parameterized with Eq. 9 as a function of τ and α. The symbols indicate the median states over open ocean and sea ice calculated for the case study on 4 April 2019. The numbers (all in $\mathrm{W\,m^{-2}}$) quantify the solar CRE change along the respective lines. The red numbers represent the contributions of τ and α to the solar CRE difference found for the evaluation point, which is given by the intersection of the black solid line connecting both states and the black dashed line, along which the solar CRE change exactly amounts to the solar CRE difference between both states.

The absolute contribution of τ or α to $\Delta\mathrm{CRE}$ is given by the partial CRE difference $\Delta\mathrm{CRE}_{\Delta\tau}(\alpha)$ or $\Delta\mathrm{CRE}_{\Delta\alpha}(\tau)$ due to a change $\Delta\tau$ or $\Delta\alpha$ between open ocean and sea ice. Due to the non-linear dependence of S_τ and S_α on both α and τ (see Fig. A1 in Appendix A), the partial CRE difference with respect to one variable is a function of the other variable (see numbers in Fig. 4). Despite an identical $\Delta\tau$, the associated CRE change is 8.3 $\mathrm{W\,m^{-2}}$ if α corresponds to the median over open ocean, but only 0.6 $\mathrm{W\,m^{-2}}$ if the median value of α over sea ice is assumed. Similarly, the CRE change due to $\Delta\alpha$ differs depending on τ, with 131.6 $\mathrm{W\,m^{-2}}$ for the median over open ocean and 124.0 $\mathrm{W\,m^{-2}}$ for the median over sea ice. In order to exactly decompose $\Delta\mathrm{CRE}$ into the partial CRE differences, with

$$\Delta\mathrm{CRE} = \Delta\mathrm{CRE}_{\Delta\tau}(\alpha_\mathrm{e}) + \Delta\mathrm{CRE}_{\Delta\alpha}(\tau_\mathrm{e}), \tag{13}$$

the evaluation point $(\alpha_\mathrm{e}, \tau_\mathrm{e})$ needs to be identified. Neither of the solutions suggested by Taylor et al. (2007) assure that the overall difference is conserved by the sum of the partial differences for an arbitrary number of variables. Thus, a different approach is used here. Since Eq. 13 is not unambiguously solvable and delivers all solutions along the black dashed line in Fig. 4, $(\alpha_\mathrm{e}, \tau_\mathrm{e})$ is retrieved as the intersection of this isoline with the straight line connecting the two states (black solid line in

https://doi.org/10.5194/egusphere-2025-1210
Preprint. Discussion started: 25 March 2025

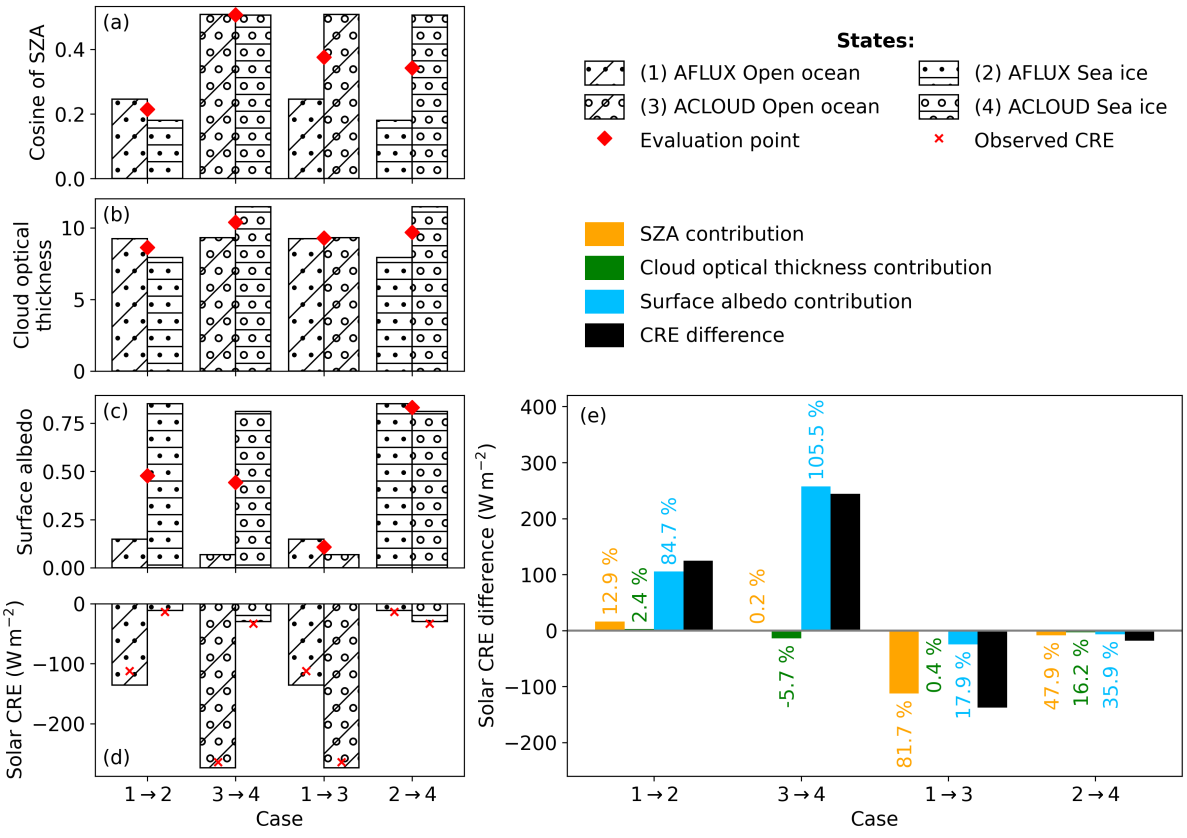

Figure 5. Median values of (a) μ, (b) τ, and (c) α and (d) the resulting solar CRE parameterized with Eq. 9 for the two states compared for the respective case. The cases are labelled such that the numbers before and after "→" correspond to the state represented by the left and right bar, respectively; see legend for the numbers assigned to each state. The red crosses in (d) denote the observed solar CRE for each state. The coordinates μ_e, τ_e, and α_e of the evaluation point obtained for each case are marked with the red diamonds in (a–c). (e) Absolute (coloured bars) and relative (numbers) contributions to the CRE difference between the states (black bar) of each case.

Fig. 4), which is parameterized as:

$$\begin{pmatrix} \tau_e \\ \alpha_e \end{pmatrix} = \begin{pmatrix} \tau_1 \\ \alpha_1 \end{pmatrix} + s \begin{pmatrix} \tau_2 - \tau_1 \\ \alpha_2 - \alpha_1 \end{pmatrix}. \tag{14}$$

The subscripts 1 and 2 refer to the two states, in this case open ocean and sea ice. Inserting Eq. 14 into Eq. 13 yields a solution for the parameter s that is used to calculate $(\alpha_e, \tau_e) = (0.49, 7.7)$. For these values, the absolute (relative) contributions of cloud and surface calculated with Eq. 13 amount to 4.3 W m^{-2} (3.3 %) and 127.9 W m^{-2} (96.7 %), respectively.

https://doi.org/10.5194/egusphere-2025-1210
Preprint. Discussion started: 25 March 2025

4.2 Application to different seasons and surface types

The method described in Sect. 4.1 can be used to quantify the contributions of the various drivers to a CRE difference between two arbitrary states. For four additional cases, this section calculates the contributions of μ, τ, and α to the CRE differences between surface types and seasonally different campaigns, which were qualitatively discussed by Becker et al. (2023). Since the SZA variation between these observations was significant, the dependence of the SZA is included in these calculations. Thus, a contribution term of μ is added to Eq. 13, such that

$$\Delta\mathrm{CRE} = \Delta\mathrm{CRE}_{\Delta\mu}(\tau_\mathrm{e}, \alpha_\mathrm{e}) + \Delta\mathrm{CRE}_{\Delta\tau}(\mu_\mathrm{e}, \alpha_\mathrm{e}) + \Delta\mathrm{CRE}_{\Delta\alpha}(\mu_\mathrm{e}, \tau_\mathrm{e}), \tag{15}$$

and the vectorial Eq. 14 now reads:

$$\begin{pmatrix} \mu_\mathrm{e} \\ \tau_\mathrm{e} \\ \alpha_\mathrm{e} \end{pmatrix} = \begin{pmatrix} \mu_1 \\ \tau_1 \\ \alpha_1 \end{pmatrix} + s \begin{pmatrix} \mu_2 - \mu_1 \\ \tau_2 - \tau_1 \\ \alpha_2 - \alpha_1 \end{pmatrix}. \tag{16}$$

For all cases and the corresponding states, the median values of μ, τ, and α, the calculated CRE and the retrieved contributions are summarized in Fig. 5. The two leftmost cases investigate the CRE difference between open ocean and sea ice for AFLUX and ACLOUD, while the remaining cases quantify the contributions between the two campaigns, separately for open ocean and sea ice. The significantly different α (Fig. 5c) dominates the CRE difference between open ocean and sea ice with a relative contribution of at least 84.7 %. Only during AFLUX, the lower SZA over open ocean compared to sea ice (75.5° vs. 79.6°) significantly contributed to the CRE difference with 12.9 %. Comparing AFLUX and ACLOUD, the seasonally different SZA (Fig. 5a) contributes most to the CRE difference, but seasonal changes in α are not negligible. Especially over sea ice, the snow albedo was decreased by melting and contributed 35.9 % to the CRE difference, while the dominant SZA contribution of 47.9 % was relatively weak. However, note that the neglect of the albedo change between cloudy and cloud-free conditions overestimated the relative contribution of α to this CRE difference. In contrast, the 17.9 % contribution of α over open ocean is likely an artifact of sea smoke below the aircraft, which increased the measured albedo during AFLUX (Becker et al., 2023). The states of all cases were dominated by optically thick clouds, to which the sensitivity of the CRE is weak (Fig. A1a in Appendix A). Therefore, the relative contributions of τ are generally low. During ACLOUD, τ negatively contributed to the CRE change due to optically thicker clouds over sea ice. The largest difference in τ occurred over sea ice between AFLUX and ACLOUD (Fig. 5b), resulting in the highest relative contribution of τ between two states with 16.2 %.

5 Conclusions

Future changes of the Arctic climate are expected to alter the properties of clouds, resulting in a modification of the cloud radiative effect (CRE). Since this CRE modification is similarly affected by concurrent changes in non-cloud properties, such as surface albedo or water vapour, separating the cloud and various non-cloud contributions composing the CRE is crucial to accurately identify, represent, and disentangle different cloud-involving interactions and their relative importances. Based on

https://doi.org/10.5194/egusphere-2025-1210
Preprint. Discussion started: 25 March 2025

Shupe and Intrieri (2004), this study developed a simple but accurate parameterization of the solar CRE, which is applied to airborne radiation observations to quantitatively investigate the impact of concurrently observed SZA, surface albedo α, and cloud optical thickness τ on the solar surface CRE. These investigations were largely based on an appropriate case study with inhomogeneous cloud and surface conditions in the vicinity of the marginal sea ice zone. Since the SZA was almost constant around 75°, its impact was negligible for this example case. For continuous observations, the impact of each parameter on the CRE evolution was determined by the absolute change of, and the sensitivity of the CRE to, the respective parameter. During the example case, the surface transition from open ocean to sea ice clearly dominated the solar CRE despite a significant intermediate cloud thickening, which was largely inefficient due to the weak CRE sensitivity on τ for optically thick clouds.

To separate the contributions between two distinct states, a method following Taylor et al. (2007) was used. For the example case, this method revealed that the contrasting surface albedo contributed more than 95 % to the solar CRE difference between open ocean and sea ice, while the cloud impact was weak. Based on observations from an airborne spring and summer campaign, the method was applied to additionally calculate relative contributions for CRE differences between different surface types and seasons. The quantified contributions confirmed the qualitative assessment of Becker et al. (2023). The solar CRE difference between open ocean and sea ice is at least 84 % due to the surface albedo contrast, while the SZA difference contributed more than half to the CRE change from spring to summer. The cloud impact itself was found to be low in all cases, corroborating the frequent dominance of non-cloud properties for the CRE. To disentangle the full impacts of cloud and non-cloud properties on the total CRE, a similar analysis for the thermal-infrared (TIR) CRE would be required. However, an as simple method is challenging due to the strong dependence of the TIR CRE on profiles of temperature, water vapour, and clouds.

Appendix A: Sensitivity of solar CRE

Based on Eqs. 11 and 12 and the fixed $\bar{\mu} = 0.264$, the sensitivities $S_\tau(\tau, \alpha)$ and $S_\alpha(\tau, \alpha)$ are calculated for a wide range of τ and α and illustrated in Fig. A1. The sensitivity of the CRE with respect to τ is negative (Fig. A1a), indicating an enhanced cooling effect with increasing τ. The CRE is particularly sensitive to optically thin clouds (τ less than 2) over open ocean, where the magnitude of S_τ generally exceeds 20 W m^{-2} per unit of τ. For the same values of τ over sea ice, S_τ is reduced due to the weaker solar cooling effect compared to open ocean. Optically thick clouds with τ larger than 10 cause a weak magnitude of S_τ, not exceeding 5 W m^{-2} per unit of τ over open ocean and 1 W m^{-2} per unit of τ over sea ice. Generally, the magnitude of S_τ increases with both decreasing τ and decreasing α.

The sensitivity of the CRE with respect to α (Fig. A1b) strengthens with increasing τ and decreasing α and the positive values express a larger CRE (weaker cooling effect) for higher α. In optically thick cloud conditions over open ocean, the CRE is particularly sensitive to surface albedo changes (S_α larger than 200 W m^{-2} per unit of α). However, clouds with τ equal to 1 are sufficient for a minimum S_α of 50 W m^{-2} per unit of α.

https://doi.org/10.5194/egusphere-2025-1210
Preprint. Discussion started: 25 March 2025

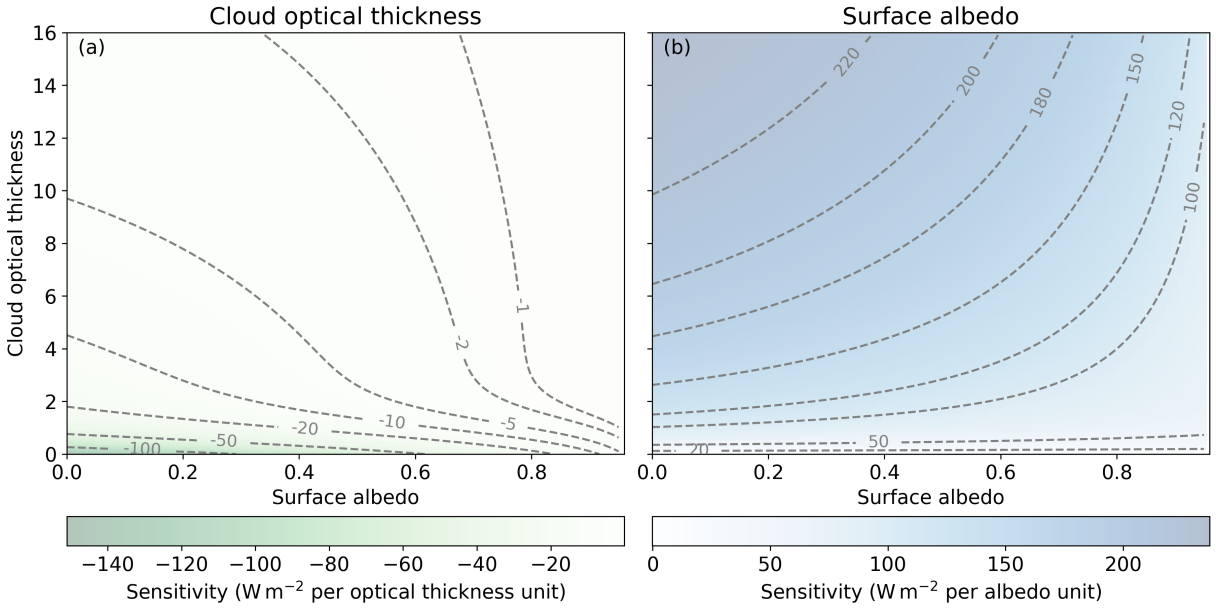

Figure A1. Sensitivity of the solar CRE with respect to (a) cloud optical thickness (S_τ) and (b) surface albedo (S_α) as a function of τ and α, calculated for the constant $\bar{\mu}$ of 0.264 (corresponding to SZA of 74.7°).

Data availability. The data analyzed in this manuscript are publically available on the PANGAEA database (Stapf et al., 2021, https://doi.pangaea.de/10.1594/PANGAEA.932010).

Author contributions. SB developed the method, analyzed the data for this study, and drafted the article. MW and AE designed the experimental basis of this study. All authors contributed to discussion and interpretation of the results and the editing of the article.

Competing interests. The authors declare that they have no conflict of interest.

Acknowledgements. We gratefully acknowledge the funding by the Deutsche Forschungsgemeinschaft (DFG, German Research Foundation) – Projektnummer 268020496 – TRR 172, within the Transregional Collaborative Research Center "ArctiC Amplification: Climate Relevant Atmospheric and SurfaCe Processes, and Feedback Mechanisms (AC)^3. This work was funded by the Open Access Publishing Fund of Leipzig University supported by the DFG within the program Open Access Publication Funding.

https://doi.org/10.5194/egusphere-2025-1210
Preprint. Discussion started: 25 March 2025

References

Becker, S., Ehrlich, A., Schäfer, M., and Wendisch, M.: Airborne observations of the surface cloud radiative effect during different seasons over sea ice and open ocean in the Fram Strait, Atmos. Chem. Phys., 23, 7015–7031, https://doi.org/10.5194/acp-23-7015-2023, 2023.

Cess, R. D., Potter, G. L., Blanchet, J. P., Boer, G. J., Del Genio, A. D., Déqué, M., Dymnikov, V., Galin, V., Gates, W. L., Ghan, S. J., Kiehl, J. T., Lacis, A. A., Le Treut, H., Li, Z., Liang, X., McAvaney, B. J., Meleshko, V. P., Mitchell, J. F. B., Morcrette, J., Randall, D. A., Rikus, L., Roeckner, E., Royer, J. F., Schlese, U., Sheinin, D. A., Slingo, A., Sokolov, A. P., Taylor, K. E., Washington, W. M., Wetherald, R. T., Yagai, I., and Zhang, M.: Intercomparison and interpretation of climate feedback processes in 19 atmospheric general circulation models, J. Geophys. Res.: Atmos., 95, 16 601–16 615, https://doi.org/10.1029/jd095id10p16601, 1990.

Choi, Y.-S., Hwang, J., Ok, J., Park, D.-S. R., Su, H., Jiang, J. H., Huang, L., and Limpasuvan, T.: Effect of Arctic clouds on the ice-albedo feedback in midsummer, Int. J. Climatol., 40, 4707–4714, https://doi.org/10.1002/joc.6469, 2020.

Cox, C. J., Walden, V. P., Rowe, P. M., and Shupe, M. D.: Humidity trends imply increased sensitivity to clouds in a warming Arctic, Nat. Commun., 6, 10 117, https://doi.org/10.1038/ncomms10117, 2015.

Di Biagio, C., di Sarra, A., Eriksen, P., Ascanius, S. E., Muscari, G., and Holben, B.: Effect of surface albedo, water vapour, and atmospheric aerosols on the cloud-free shortwave radiative budget in the Arctic, Climate Dynamics, 39, 953–969, https://doi.org/10.1007/s00382-011-1280-1, 2012.

Ebell, K., Nomokonova, T., Maturilli, M., and Ritter, C.: Radiative Effect of Clouds at Ny-Ålesund, Svalbard, as Inferred from Ground-Based Remote Sensing Observations, J. Appl. Meteorol. Climatol., 59, 3–22, https://doi.org/10.1175/jamc-d-19-0080.1, 2020.

Ehrlich, A., Wendisch, M., Lüpkes, C., Buschmann, M., Bozem, H., Chechin, D., Clemen, H.-C., Dupuy, R., Eppers, O., Hartmann, J., Herber, A., Jäkel, E., Järvinen, E., Jourdan, O., Kästner, U., Kliesch, L.-L., Köllner, F., Mech, M., Mertes, S., Neuber, R., Ruiz-Donoso, E., Schnaiter, M., Schneider, J., Stapf, J., and Zanatta, M.: A comprehensive in situ and remote sensing data set from the Arctic CLoud Observations Using airborne measurements during polar Day (ACLOUD) campaign, Earth Syst. Sci. Data, 11, 1853–1881, https://doi.org/10.5194/essd-11-1853-2019, 2019.

Emde, C., Buras-Schnell, R., Kylling, A., Mayer, B., Gasteiger, J., Hamann, U., Kylling, J., Richter, B., Pause, C., Dowling, T., and Bugliaro, L.: The libRadtran software package for radiative transfer calculations (version 2.0.1), Geosci. Model Dev., 9, 1647–1672, https://doi.org/10.5194/gmd-9-1647-2016, 2016.

Fitzpatrick, M. F., Brandt, R. E., and Warren, S. G.: Transmission of Solar Radiation by Clouds over Snow and Ice Surfaces: A Parameterization in Terms of Optical Depth, Solar Zenith Angle, and Surface Albedo, J. Climate, 17, 266–275, https://doi.org/10.1175/1520-0442(2004)017<0266:tosrbc>2.0.co;2, 2004.

Forster, P., Storelvmo, T., Armour, K., Collins, W., Dufresne, J.-L., Frame, D., Lunt, D., Mauritsen, T., Palmer, M., Watanabe, M., Wild, M., and Zhan, H.: The Earth's Energy Budget, Climate Feedbacks, and Climate Sensitivity, in: Climate Change 2021: The Physical Science Basis. Contribution of Working Group I to the Sixth Assessment Report of the Intergovernmental Panel on Climate Change, edited by Masson-Delmotte, V., Zhai, P., Pirani, A., Connors, S., Péan, C., Berger, S., Caud, N., Chen, Y., Goldfarb, L., Gomis, M., Huang, M., Leitzell, K., Lonnoy, E., Matthews, J., Maycock, T., Waterfield, T., Yelekçi, O., Yu, R., and Zhou, B., book section 9, pp. 923–1054, Cambridge University Press, Cambridge, United Kingdom and New York, NY, USA, https://doi.org/10.1017/9781009157896.009, 2021.

Gardner, A. S. and Sharp, M. J.: A review of snow and ice albedo and the development of a new physically based broadband albedo parameterization, J. Geophys. Res., 115, F01 009, https://doi.org/10.1029/2009jf001444, 2010.

https://doi.org/10.5194/egusphere-2025-1210
Preprint. Discussion started: 25 March 2025

Goosse, H., Kay, J. E., Armour, K. C., Bodas-Salcedo, A., Chepfer, H., Docquier, D., Jonko, A., Kushner, P. J., Lecomte, O., Massonnet, F., Park, H.-S., Pithan, F., Svensson, G., and Vancoppenolle, M.: Quantifying climate feedbacks in polar regions, Nature Communications, 9, https://doi.org/10.1038/s41467-018-04173-0, 2018.

Hall, A.: The Role of Surface Albedo Feedback in Climate, J. Climate, 17, 1550–1568, https://doi.org/10.1175/1520-0442(2004)017<1550:trosaf>2.0.co;2, 2004.

Hersbach, H., Bell, B., Berrisford, P., Hirahara, S., Horányi, A., Muñoz-Sabater, J., Nicolas, J., Peubey, C., Radu, R., Schepers, D., Simmons, A., Soci, C., Abdalla, S., Abellan, X., Balsamo, G., Bechtold, P., Biavati, G., Bidlot, J., Bonavita, M., Chiara, G. D., Dahlgren, P., Dee, D., Diamantakis, M., Dragani, R., Flemming, J., Forbes, R., Fuentes, M., Geer, A., Haimberger, L., Healy, S., Hogan, R. J., Hólm, E., Janisková, M., Keeley, S., Laloyaux, P., Lopez, P., Lupu, C., Radnoti, G., de Rosnay, P., Rozum, I., Vamborg, F., Villaume, S., and Thépaut, J.-N.: The ERA5 global reanalysis, Q. J. Roy. Meteor. Soc., 146, 1999–2049, https://doi.org/10.1002/qj.3803, 2020.

Intrieri, J. M., Fairall, C. W., Shupe, M. D., Persson, P. O. G., Andreas, E. L., Guest, P. S., and Moritz, R. E.: An annual cycle of Arctic surface cloud forcing at SHEBA, J. Geophys. Res., 107, https://doi.org/10.1029/2000jc000439, 2002.

Jäkel, E., Sperzel, T. R., Wendisch, M., Wolf, K., Lampert, A., Birnbaum, G., and Dorn, W.: What drives the Arctic solar radiative energy budget at the surface – clouds or surface albedo?, submitted to J. Eur. Meteorol. Soc., 2024.

Jin, Z., Qiao, Y., Wang, Y., Fang, Y., and Yi, W.: A new parameterization of spectral and broadband ocean surface albedo, Opt. Express, 19, 26 429–26 443, https://doi.org/10.1364/oe.19.026429, 2011.

Kay, J. E., L'Ecuyer, T., Chepfer, H., Loeb, N., Morrison, A., and Cesana, G.: Recent Advances in Arctic Cloud and Climate Research, Curr. Clim. Change Rep., 2, 159–169, https://doi.org/10.1007/s40641-016-0051-9, 2016.

Mech, M., Ehrlich, A., Herber, A., Lüpkes, C., Wendisch, M., Becker, S., Boose, Y., Chechin, D., Crewell, S., Dupuy, R., Gourbeyre, C., Hartmann, J., Jäkel, E., Jourdan, O., Kliesch, L.-L., Klingebiel, M., Kulla, B. S., Mioche, G., Moser, M., Risse, N., Ruiz-Donoso, E., Schäfer, M., Stapf, J., and Voigt, C.: MOSAiC-ACA and AFLUX - Arctic airborne campaigns characterizing the exit area of MOSAiC, Sci. Data, 9, https://doi.org/10.1038/s41597-022-01900-7, 2022.

Meier, W. N., Petty, A., Hendricks, S., Perovich, D., Farrell, S., Webster, M., Divine, D., Gerland, S., Kaleschke, L., Ricker, R., and Tian-Kunze, X.: Sea Ice, in: NOAA Arctic Report Card 2022, edited by M. L. Druckenmiller and R. L. Thoman and T. A. Moon, Global Ocean Monitoring and Observing (U.S.), https://doi.org/10.25923/xyp2-vz45, 2022.

Miller, N. B., Shupe, M. D., Cox, C. J., Walden, V. P., Turner, D. D., and Steffen, K.: Cloud Radiative Forcing at Summit, Greenland, J. Climate, 28, 6267–6280, https://doi.org/10.1175/jcli-d-15-0076.1, 2015.

Mioche, G., Jourdan, O., Delanoë, J., Gourbeyre, C., Febvre, G., Dupuy, R., Monier, M., Szczap, F., Schwarzenboeck, A., and Gayet, J.-F.: Vertical distribution of microphysical properties of Arctic springtime low-level mixed-phase clouds over the Greenland and Norwegian seas, Atmos. Chem. Phys., 17, 12 845–12 869, https://doi.org/10.5194/acp-17-12845-2017, 2017.

Morrison, A. L., Kay, J. E., Frey, W. R., Chepfer, H., and Guzman, R.: Cloud Response to Arctic Sea Ice Loss and Implications for Future Feedback in the CESM1 Climate Model, J. Geophys. Res.: Atmos., 124, 1003–1020, https://doi.org/10.1029/2018jd029142, 2019.

Perovich, D. K., Tucker, W. B., and Ligett, K. A.: Aerial observations of the evolution of ice surface conditions during summer, J. Geophys. Res.: Oceans, 107, https://doi.org/10.1029/2000jc000449, 2002.

Ramanathan, V., Cess, R. D., Harrison, E. F., Minnis, P., Barkstrom, B. R., Ahmad, E., and Hartmann, D.: Cloud-Radiative Forcing and Climate: Results from the Earth Radiation Budget Experiment, Science, 243, 57–63, https://doi.org/10.1126/science.243.4887.57, 1989.

Serreze, M. C. and Barry, R. G.: Processes and impacts of Arctic amplification: A research synthesis, Global Planet. Change, 77, 85–96, https://doi.org/10.1016/j.gloplacha.2011.03.004, 2011.

https://doi.org/10.5194/egusphere-2025-1210
Preprint. Discussion started: 25 March 2025

Shell, K. M., Kiehl, J. T., and Shields, C. A.: Using the Radiative Kernel Technique to Calculate Climate Feedbacks in NCAR's Community Atmospheric Model, J. Climate, 21, 2269–2282, https://doi.org/10.1175/2007jcli2044.1, 2008.

Shupe, M. D. and Intrieri, J. M.: Cloud Radiative Forcing of the Arctic Surface: The Influence of Cloud Properties, Surface Albedo, and Solar Zenith Angle, J. Climate, 17, 616–628, https://doi.org/10.1175/1520-0442(2004)017<0616:crfota>2.0.co;2, 2004.

Soden, B. J., Broccoli, A. J., and Hemler, R. S.: On the Use of Cloud Forcing to Estimate Cloud Feedback, J. Climate, 17, 3661–3665, https://doi.org/10.1175/1520-0442(2004)017<3661:otuocf>2.0.co;2, 2004.

Soden, B. J., Held, I. M., Colman, R., Shell, K. M., Kiehl, J. T., and Shields, C. A.: Quantifying Climate Feedbacks Using Radiative Kernels, J. Climate, 21, 3504–3520, https://doi.org/10.1175/2007jcli2110.1, 2008.

Spreen, G., Kaleschke, L., and Heygster, G.: Sea ice remote sensing using AMSR-E 89-GHz channels, J. Geophys. Res., 113, C02S03, https://doi.org/10.1029/2005jc003384, 2008.

Stapf, J., Ehrlich, A., Jäkel, E., Lüpkes, C., and Wendisch, M.: Reassessment of shortwave surface cloud radiative forcing in the Arctic: consideration of surface-albedo–cloud interactions, Atmos. Chem. Phys., 20, 9895–9914, https://doi.org/10.5194/acp-20-9895-2020, 2020.

Stapf, J., Ehrlich, A., and Wendisch, M.: Cloud radiative forcing, LWP and cloud-free albedo derived from airborne broadband irradiance observations during the AFLUX and ACLOUD campaign, PANGAEA [data set], https://doi.org/10.1594/PANGAEA.932010, 2021.

Taylor, K. E., Crucifix, M., Braconnot, P., Hewitt, C. D., Doutriaux, C., Broccoli, A. J., Mitchell, J. F. B., and Webb, M. J.: Estimating Shortwave Radiative Forcing and Response in Climate Models, J. Climate, 20, 2530–2543, https://doi.org/10.1175/jcli4143.1, 2007.

Uttal, T., Curry, J. A., Mcphee, M. G., Perovich, D. K., Moritz, R. E., Maslanik, J. A., Guest, P. S., Stern, H. L., Moore, J. A., Turenne, R., Heiberg, A., Serreze, M. C., Wylie, D. P., Persson, O. G., Paulson, C. A., Halle, C., Morison, J. H., Wheeler, P. A., Makshtas, A., Welch, H., Shupe, M. D., Intrieri, J. M., Stamnes, K., Lindsey, R. W., Pinkel, R., Pegau, W. S., Stanton, T. P., and Grenfeld, T. C.: Surface Heat Budget of the Arctic Ocean, Bull. Am. Meteorol. Soc., 83, 255–275, https://doi.org/10.1175/1520-0477(2002)083<0255:shbota>2.3.co;2, 2002.

Vavrus, S. J., Bhatt, U. S., and Alexeev, V. A.: Factors Influencing Simulated Changes in Future Arctic Cloudiness, J. Clim., 24, 4817–4830, https://doi.org/10.1175/2011jcli4029.1, 2011.

Wendisch, M., Macke, A., Ehrlich, A., Lüpkes, C., Mech, M., Chechin, D., Dethloff, K., Velasco, C. B., Bozem, H., Brückner, M., Clemen, H.-C., Crewell, S., Donth, T., Dupuy, R., Ebell, K., Egerer, U., Engelmann, R., Engler, C., Eppers, O., Gehrmann, M., Gong, X., Gottschalk, M., Gourbeyre, C., Griesche, H., Hartmann, J., Hartmann, M., Heinold, B., Herber, A., Herrmann, H., Heygster, G., Hoor, P., Jafariserajehlou, S., Jäkel, E., Järvinen, E., Jourdan, O., Kästner, U., Kecorius, S., Knudsen, E. M., Köllner, F., Kretzschmar, J., Lelli, L., Leroy, D., Maturilli, M., Mei, L., Mertes, S., Mioche, G., Neuber, R., Nicolaus, M., Nomokonova, T., Notholt, J., Palm, M., van Pinxteren, M., Quaas, J., Richter, P., Ruiz-Donoso, E., Schäfer, M., Schmieder, K., Schnaiter, M., Schneider, J., Schwarzenböck, A., Seifert, P., Shupe, M. D., Siebert, H., Spreen, G., Stapf, J., Stratmann, F., Vogl, T., Welti, A., Wex, H., Wiedensohler, A., Zanatta, M., and Zeppenfeld, S.: The Arctic Cloud Puzzle: Using ACLOUD/PASCAL Multiplatform Observations to Unravel the Role of Clouds and Aerosol Particles in Arctic Amplification, Bull. Am. Meteorol. Soc., 100, 841–871, https://doi.org/10.1175/bams-d-18-0072.1, 2019.

Wendisch, M., Brückner, M., Crewell, S., Ehrlich, A., Notholt, J., Lüpkes, C., Macke, A., Burrows, J. P., Rinke, A., Quaas, J., Maturilli, M., Schemann, V., Shupe, M. D., Akansu, E. F., Barrientos-Velasco, C., Bärfuss, K., Blechschmidt, A.-M., Block, K., Bougoudis, I., Bozem, H., Böckmann, C., Bracher, A., Bresson, H., Bretschneider, L., Buschmann, M., Chechin, D. G., Chylik, J., Dahlke, S., Deneke, H., Dethloff, K., Donth, T., Dorn, W., Dupuy, R., Ebell, K., Egerer, U., Engelmann, R., Eppers, O., Gerdes, R., Gierens, R., Gorodetskaya, I. V., Gottschalk, M., Griesche, H., Gryanik, V. M., Handorf, D., Harm-Altstädter, B., Hartmann, J., Hartmann, M., Heinold, B., Herber, A., Herrmann, H., Heygster, G., Höschel, I., Hofmann, Z., Hölemann, J., Hünerbein, A., Jafariserajehlou, S., Jäkel, E., Jacobi, C., Janout,

https://doi.org/10.5194/egusphere-2025-1210
Preprint. Discussion started: 25 March 2025

M., Jansen, F., Jourdan, O., Jurányi, Z., Kalesse-Los, H., Kanzow, T., Käthner, R., Kliesch, L. L., Klingebiel, M., Knudsen, E. M., Kovács, T., Körtke, W., Krampe, D., Kretzschmar, J., Kreyling, D., Kulla, B., Kunkel, D., Lampert, A., Lauer, M., Lelli, L., von Lerber, A., Linke, O., Löhnert, U., Lonardi, M., Losa, S. N., Losch, M., Maahn, M., Mech, M., Mei, L., Mertes, S., Metzner, E., Mewes, D., Michaelis, J., Mioche, G., Moser, M., Nakoudi, K., Neggers, R., Neuber, R., Nomokonova, T., Oelker, J., Papakonstantinou-Presvelou, I., Pätzold, F., Pefanis, V., Pohl, C., van Pinxteren, M., Radovan, A., Rhein, M., Rex, M., Richter, A., Risse, N., Ritter, C., Rostosky, P., Rozanov, V. V., Donoso, E. R., Garfias, P. S., Salzmann, M., Schacht, J., Schäfer, M., Schneider, J., Schnierstein, N., Seifert, P., Seo, S., Siebert, H., Soppa, M. A., Spreen, G., Stachlewska, I. S., Stapf, J., Stratmann, F., Tegen, I., Viceto, C., Voigt, C., Vountas, M., Walbröl, A., Walter, M., Wehner, B., Wex, H., Willmes, S., Zanatta, M., and Zeppenfeld, S.: Atmospheric and Surface Processes, and Feedback Mechanisms Determining Arctic Amplification: A Review of First Results and Prospects of the $(AC)^3$ Project, Bull. Am. Meteorol. Soc., 104, E208–E242, https://doi.org/10.1175/bams-d-21-0218.1, 2023.

Wetherald, R. T. and Manabe, S.: Cloud Feedback Processes in a General Circulation Model, J. Atmo. Sci., 45, 1397–1416, https://doi.org/10.1175/1520-0469(1988)045<1397:cfpiag>2.0.co;2, 1988.